

Co-designing Transmon devices for control with simple pulses

Nicolas Wittler,^{1,2} Shai Machnes,³ and Frank K. Wilhelm^{1,2}

¹*Theoretical Physics, Saarland University, 66123 Saarbrücken, Germany*

²*Peter Grünberg Institut – Quantum Computing Analytics (PGI-12),*

*Forschungszentrum Jülich, 52425 Jülich, Germany**

³*Qruise GmbH, 66113, Saarbrücken, Germany*

(Dated: October 14, 2024)

In the current NISQ era, there is demand for functional quantum devices to solve relevant computational problems, which motivates a utilitarian perspective on device design: The goal is to create a device that is able to run a given algorithm with state-of-the-art performance. In this work, we use optimal control tools to derive the gate set required by a toy algorithm and, in tandem, explore the model space of superconducting quantum computer design, from dispersively coupled to stronger interacting qubits, to maximize gate fidelity. We employ perfect entangler theory to provide flexibility in the search for a two-qubit gate on a given platform and to compare designs with different entangling mechanisms, e.g., CPHASE and \sqrt{i} SWAP. To ensure the applicability of our investigation, we limit ourselves to "simple" (i.e., sparse parametrization) pulses and quantify, where results differ from using the full complexity of piecewise constant controls.

I. INTRODUCTION

When designing control layouts for superconducting quantum computing devices, different approaches are being pursued. Some designs, e.g., from IBM, are trying to achieve as much as is possible with fixed-frequency qubits with microwave controls, avoiding the extra noise introduced by flux lines. This has the challenge of no control over operating sweet spots and couplings after fabrication. Adding flux lines incurs the cost of increased decoherence to be able to move the working points of qubits around at will. Following this design, adding additional tunable junctions to the chip to act as couplers between data qubit junctions increases the footprint of the chip, but promises to provide controlled interactions. In addition, this isolates the data qubits from flux noise [1].

Creating devices that are well suited for a given task, as opposed to more general, fundamental research, is desirable for the practical work on quantum algorithms. To this end, tools are created to explore and fine-tune quantum device designs in an integrated manner [2–5].

It is our goal to systematically analyze designs for quantum computing devices that are fabricated for the purpose of executing quantum circuits or algorithms. We will present our procedure with the examples of two common design layouts: fixed qubits with fixed interaction (FQ), fixed qubits with a tunable coupler (TC). In this work, we'll consider the quantized Hamiltonian parameters – Transmon resonance frequencies, anharmonicities, coupling strengths – as the search space. Other efforts look to directly designing circuit quantities like charging and junction energies [4, 6] to produce devices with given properties, e.g. certain types of many qubit interaction terms.

Recent demonstrations have shown that even in restrictive control settings, almost all known gates are realiz-

able [7]. This already presents a number of permutations of control schemes and platforms that need to be evaluated. Providing a level playing field is a non-trivial task, especially when trying to distill everything into a general procedure. Targeting a generalized perfect entangler can result in better outcomes than the "textbook" two-qubit gate [8–10]. When building a device for a certain application, there's an advantage in considering the requirements this poses to the gate-set [11, 12].

This is more relevant when we add the model parameters to the search. In [13], the authors coin the term "straddling" regime – the border between dispersive and strongly coupled – and show that this regime is optimal when employing full optimal control theory. We will employ these methods to investigate the advantage of a tunable coupler setup over fixed-frequency qubits, while limiting the control capabilities to simple pulses with few parameters. We'll see what the effect of limiting the pulse complexity has on the resulting model regime.

In Section II, we reproduce some of the theory for creating entanglement. We present a general method to search for models that facilitate both entangling and local gates. As an initial application, we apply the method in Section III to a two-qubit chip with and without an extra qubit to act as a tunable coupler.

II. METHOD

For a functional quantum device, the fundamental tasks are: (1) Define and optimize local gates, (2) Define and optimize entangling gates, (3) Find optimal system parameters to achieve both types of gates to high fidelity.

This presents a priori some conflicting interests: Entangling gates naturally profit from strong coupling, as opposed to local gates, which benefit from isolating subsystems. If the target is to run quantum circuits with high accuracy, we'll need to find a compromise. Here, we will present a procedure to achieve this, based on optimal

* Corresponding author: n.wittler@pm.me

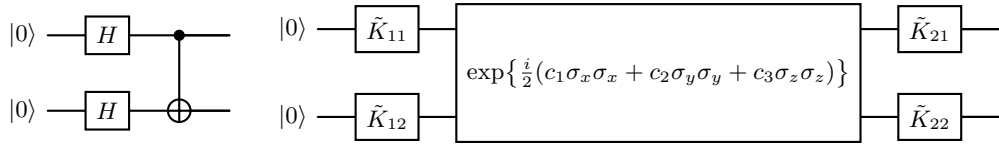


FIG. 1. **Interpreting Lie group decomposition as circuit decomposition.** (a) Typical cell of a quantum computing circuit. (b) Decomposition with arbitrary entangling gate, given by the Weyl coordinates and modified local gates \tilde{K}_{ij} . Note that in a full algorithm circuit, layers of single-qubit gates can be compressed.

control techniques.

The mechanism to generate entanglement for two-qubit gates generally depends on the platform, so choosing a perfect entangler as the optimization target is desirable to not limit possible solutions to a specific gate. For each setup, there exists a procedure to derive entangling gates; the cross-resonance (CR) gate for FQ and CPHASE or \sqrt{i} SWAP for FQ and TQ, with AC or DC controls [14–16].

A. Perfect entangler theory

A known approach is to consider an operator $U \in SU(4)$ (the computational subspace, ignoring leakage levels for now) and characterize its non-local properties by computing the Makhlin invariants g_1, g_2 and g_3 [17].

We are representing a general gate U in the Bell basis as $U_B = Q^T U Q$, where

$$Q = \frac{1}{\sqrt{2}} \begin{pmatrix} 1 & 0 & 0 & i \\ 0 & i & 1 & 0 \\ 0 & i & -1 & 0 \\ 1 & 0 & 0 & -i \end{pmatrix}. \quad (1)$$

In this basis, non-local gates are diagonal and local gates are orthogonal matrices.

The Makhlin invariants are then defined as

$$\begin{aligned} g_1 &= \text{Re} \frac{\text{Tr}(U_B^T U_B)^2}{16 \det(U)} \\ g_2 &= \text{Im} \frac{\text{Tr}(U_B^T U_B)^2}{16 \det(U)} \\ g_3 &= \frac{\text{Tr}(U_B^T U_B)^2 - \text{Tr}((U_B^T U_B)^2)}{4 \det(U)}. \end{aligned} \quad (2)$$

These invariants characterize equivalence classes, e.g., CNOT, CPHASE and CR share the same invariants, meaning they can be transformed into each other with local gates.

We can generalize further by combining the invariants $\vec{g} = (g_1, g_2, g_3)$ into a single functional,

$$d(\vec{g}) = g_3 \sqrt{g_1^2 + g_2^2} - g_1, \quad (3)$$

which vanishes for the invariants on the surface of the perfect entangler volume. Inside the volume, the value has to be set to 0 manually [18].

This functional is straightforward to compute for a given unitary and represents a general measure for entangling performance. Some care must be taken though, depending on which side of the volume the current \bar{U} lies. We are interested in comparing the performance of single and two-qubit operations during optimization and thus would prefer an equivalent fidelity of the form $|\text{Tr}\{V^\dagger \bar{U}\} / \dim V|^2$, where V is the target gate and \bar{U} the time evolution of the controlled system. One method is to use the perfect entangler functional for optimization and then evaluate the final performance based on fidelity. Since we aim to find suitable model parameters for both single-qubit and entangling gates at the same time, we propose a direct numerical approach, the "tugboat" strategy.

B. Tugboat optimization for perfect entanglers

We write a general ideal target gate using the Cartan decomposition $V = K_1 A K_2$ with

$$A = \exp\left\{\frac{i}{2}(c_1 \sigma_x \sigma_x + c_2 \sigma_y \sigma_y + c_3 \sigma_z \sigma_z)\right\} \quad (4)$$

where $K_{1,2} \in SU(2) \otimes SU(2)$. It can be shown, e.g., in [19], that the subalgebra $\{\sigma_x \sigma_x, \sigma_y \sigma_y, \sigma_z \sigma_z\}$ is sufficient to generate all of $SU(4)$ when combined with local rotations $K_{1,2}$. As an example, $\sigma_x \sigma_y$ can be realized from $\sigma_x \sigma_x$ by a single-qubit $\mathbb{1} \sigma_z$.

If we now confine the Weyl coordinates c_i to the volume of perfect entanglers (shaded blue in Fig. 2), we have a recipe to explicitly construct an arbitrary entangling gate. To this end, we propose the coordinate transformation

$$\begin{aligned} c_1 &= \frac{b_1 + b_2}{2} \\ c_2 &= \frac{b_1 - b_2}{2} \\ c_3 &= b_3(\pi/4 - |c_2 - \pi/4|) \end{aligned} \quad (5)$$

to conveniently express the boundary conditions for the perfect entangler volume [8] as

$$\begin{aligned} \pi/4 &\leq b_1 \leq \pi/2 \\ 0 &\leq b_2 \leq \pi/4 \\ 0 &\leq b_3 \leq \pi. \end{aligned} \quad (6)$$

We will now consider a target gate, the "tugboat", $V(\vec{\gamma}, \vec{b})$, where $\vec{b} = (b_i)$ are the transformed Weyl coordinates, confined to the volume of perfect entanglers, and local rotations $\vec{\gamma} = (\gamma_i^{(j)})$ with $j = 1, 2$ enumerating the qubits and $i = x, y, z$ the rotation axis.

We assign an explicit fidelity error to a quantum gate \bar{U} as

$$\epsilon_{\text{II}}(\bar{U}) = \min_{\vec{b}, \vec{\gamma}} \left\{ 1 - \left| \text{Tr} \left\{ V^\dagger(\vec{b}, \vec{\gamma}) \bar{U} \right\} / \dim V \right|^2 \right\} \quad (7)$$

where \bar{U} is the time evolution of the system, projected into the computational subspace. It is not resource intensive to compute a unitary matrix V in this representation, compared to the system time evolution \bar{U} which requires several orders more computational power. We can thus easily find the closest perfect entangler representation to the implemented gate \bar{U} by varying \vec{b} and $\vec{\gamma}$ at each optimization step. This way we assign a regular fidelity measure to \bar{U} while retaining the generality of the perfect entangler goal. An added benefit of this procedure is that we also explicitly extract the Weyl coordinates and local rotations of the entangling gate that allow us to identify the equivalence class.

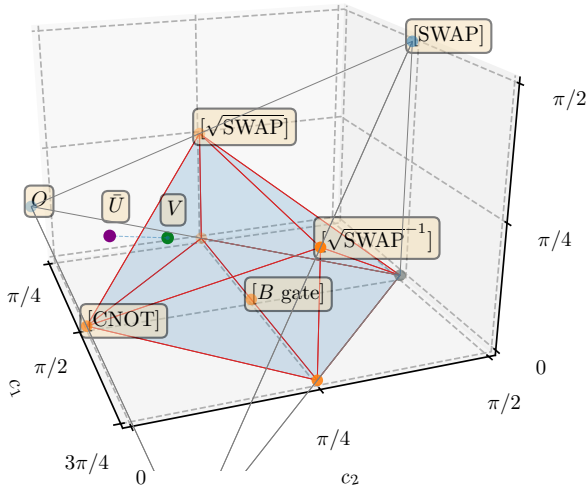


FIG. 2. **Weyl chamber of named gates to illustrate the optimization procedure.** The labeled points indicate equivalence classes with respect to local rotations. The system dynamics \bar{U} (projected into the computational space) are steered by the control and model parameters, while the target gate V is varied over the shaded volume, bounded by Eq. (6). This enables us to use $\left| \text{Tr} \left\{ V^\dagger(\vec{b}, \vec{\gamma}) \bar{U} \right\} \right|$ in a regular distance measure Eq. (7), indicated by the dashed line.

C. Optimal co-design

In this formalism, we can now also explore the model parameter space by including it in the optimization. Assume the model is described by a Hamiltonian $H(\vec{\alpha}, \vec{\beta})$, with $\vec{\beta}$ being the vector of model parameters and $\vec{\alpha}$ the controls. The system dynamics are then given by

$$U(\vec{\alpha}, \vec{\beta}) = \mathcal{T} \exp \left\{ -\frac{i}{\hbar} \int dt H(\vec{\alpha}, \vec{\beta}) \right\} \quad (8)$$

so formally the goal function depends on $\epsilon_{\text{II}} \equiv \epsilon_{\text{II}}(\vec{\alpha}, \vec{\beta}, \vec{b}, \vec{\gamma})$.

Textbook representations of two-qubit gates, e.g. CNOT = $|0\rangle\langle 0| \mathbb{1} + |1\rangle\langle 1| \sigma_x$, are implicitly written in the interaction picture according to the Hamiltonian in the measurement basis, denoted as \tilde{H} . We'll consider the readout basis to be the eigenbasis of the undriven system.

We obtain the time evolution $\bar{U} = \mathcal{T} \exp(-i \int H dt)$ in the product basis, since this basis will not change when we tune system parameters. Depending on the parameter regime, writing the transformation that diagonalizes H is not straightforward enough to facilitate computing the gradient of the goal function with respect to model properties.

To evaluate the optimization results for fixed parameters, we can simulate $\tilde{H} = S^\dagger H S$, the diagonal (if applicable, dressed) Hamiltonian. We then write the goal unitary as $G = S \tilde{G} S^\dagger$ and, finally, the goal function as

$$\epsilon = 1 - \left| \frac{1}{\dim G} \text{Tr} \{ G^\dagger \bar{U} \} \right|^2 \quad (9)$$

We can use $S \equiv S(\beta)$, the closed, exact form in the computational subspace, that is dependent on ω_1, ω_2 and g .

$$S = \begin{pmatrix} \cos(b) & 0 & 0 & \sin(b) \\ 0 & \cos(a) & \sin(a) & 0 \\ 0 & \sin(a) & \cos(a) & 0 \\ -\sin(b) & 0 & 0 & \cos(b) \end{pmatrix} \quad (10)$$

with $a = \arctan\left(\frac{g}{\omega_2 - \omega_1}\right)$ rotating the exchange interaction and $b = \arctan\left(\frac{g}{\omega_2 + \omega_1}\right)$ rotating the double excitations. Since we performed the RWA on the interaction terms, here $b = 0$.

As the fidelity of consecutive quantum gates is given by their product, the error for single-qubit gates (ϵ_{I}) followed by an entangling gate (with error ϵ_{II}) is

$$\bar{\epsilon} = 1 - (1 - \epsilon_{\text{I}})(1 - \epsilon_{\text{II}}) = \epsilon_{\text{I}} + \epsilon_{\text{II}} - \epsilon_{\text{I}}\epsilon_{\text{II}} \quad (11)$$

where we'll neglect the product $\epsilon_{\text{I}}\epsilon_{\text{II}}$ as its contribution is small for errors below 1% and use $\epsilon = \epsilon_{\text{I}} + \epsilon_{\text{II}}$ as our goal function.

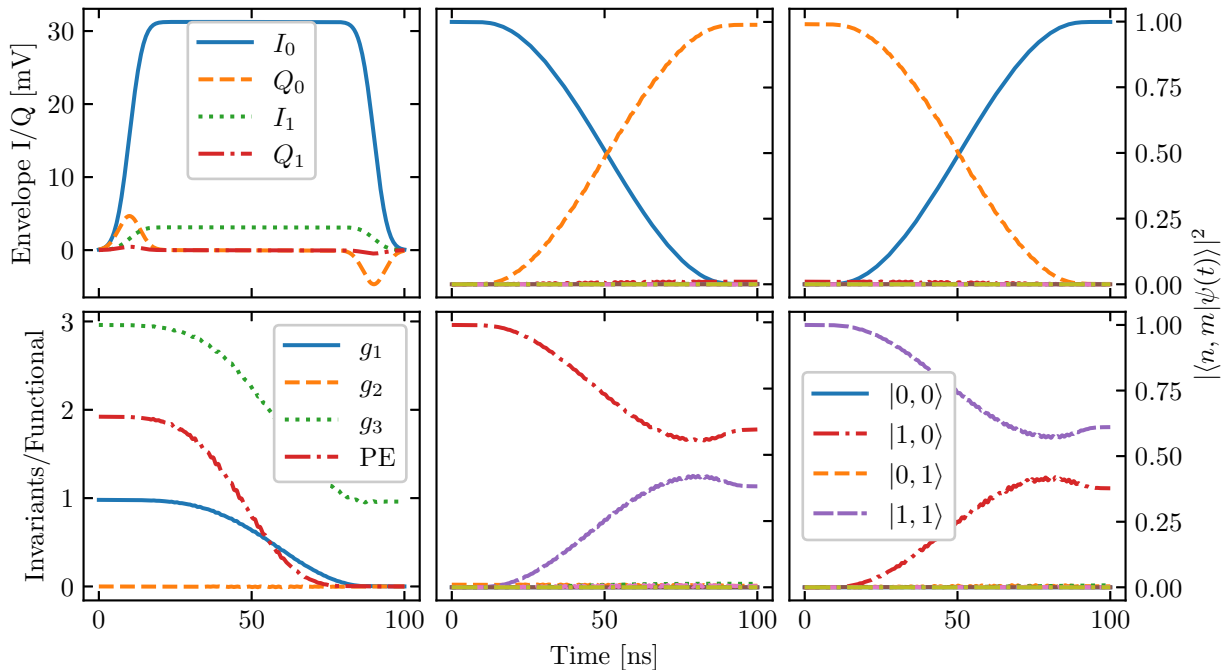


FIG. 3. **Control fields and time-evolution of computational state populations of the two fixed Transmon device.** Both control fields are on resonance with the bare frequency of the second Transmon and the amplitude of the drive is increased by $(\omega_2 - \omega_1)/g$. Their I and Q envelopes are shown on the top left. The panels on the right show the time evolution of populations, initialized in the four computational basis states. We observe a Rabi oscillation for Transmon 2 (right index, the *target*), when Transmon 1 (left index, the *control*) is in the 0 state. When the control Transmon is in the 1 state, only a partial population transfer occurs at a higher general Rabi frequency, realizing a general cross-resonance effect. To verify the entangling property, we plot the Makhlin invariants and the value of the perfect entangler (PE) functional from Eq. (3).

III. APPLICATION

We now apply the co-design procedure to explore designs for superconducting qubits. Model space consists of two Transmons with frequencies $\omega_{1,2}$, anharmonicities $\alpha_{1,2}$ and static interaction g collected in a five-dimensional vector $\vec{\beta} = (\omega_1, \omega_2, \alpha_1, \alpha_2, g)$. From the formal perspective, optimizing both model and controls at the same time constitutes a form of over-parametrization. For example, changes in drive tone and qubit frequency have the same effect on the goal function. Thus, we opt for simple controls, as opposed to a more general piecewise constant parametrization with hundreds of samples, so that the dimensions of $\vec{\alpha}$ and $\vec{\beta}$ are in the same order of magnitude.

We will first run through the process for the two-qubit chip with fixed interaction strength, and then add a third qubit to act as a tunable coupler. To characterize the model by a single number, we take the reduced coupling $\chi = g_{12}/(\omega_2 - \omega_1)$ and use the "straddling" regime $\chi = 0.1$ as a divider between the dispersive ($\chi < 0.1$) and strong coupling ($\chi > 0.1$). When there is a tunable coupler, we use the effective interaction strength, where the coupler is adiabatically eliminated to have a comparable quantity [20].

A. Local vs. entangling gates

For universal quantum computing, we need to derive a set of local, single-qubit gates and an entangling gate. As a first application, we consider a device made up of two fixed-frequency Transmons with a static coupling. With all driving and coupling resonators eliminated, the Hamiltonian is $H = \sum_{j=0,1,2,g} H_j$ with

$$\begin{aligned} H_0 &= \sum_i \omega_i a_i^\dagger a_i + \frac{\delta_i}{2} (a_i^\dagger a_i - 1) a_i^\dagger a_i \\ H_g &= g (a_1^\dagger a_2 + a_1 a_2^\dagger) \\ H_i &= u_i(\vec{\alpha}, t) (a_i^\dagger + a_i), \end{aligned} \quad (12)$$

where we are just considering the exchange interaction.

The control field on qubit i is $u(\vec{\alpha}, t) = A [I_i(t) \cos(\omega_i^d t + \phi_i) + Q_i(t) \sin(\omega_i^d t + \phi_i)]$ with a slow-varying, envelope I_i . As a basis function, we choose a flattop Gaussian shape

$$I_i(t) = \text{erf}\left(-\frac{(t - t_{\text{up}})}{\sigma}\right) - \text{erf}\left(\frac{(t - t_{\text{down}})}{\sigma}\right) \quad (13)$$

with amplitude A_i and ramps at t_{up} and t_{down} with a fixed width $\sigma = 5$ ns. We also add an out-of-phase DRAG [21] correction as $Q_i = \lambda_i \partial_t I_i$.

First, we optimize both controls $\vec{\alpha} = (A_i, \omega_i, \phi_i, t_{\text{up}}^i, t_{\text{down}}^i, \lambda_i)$ and model parameters $\vec{\beta} = (\omega_i, \delta_i, g)$ to find single-qubit gates. We characterize the system by its reduced coupling strength $g/(\omega_2 - \omega_1)$. To find the entangling gate, we employ the procedure described in Section II B. In Fig. 3 we show some example dynamics. We initialize the target gate V centered in the volume of perfect entanglers at $\vec{c}/\pi = (1/2, 1/4, 0.05)$ and the local rotations $\vec{\gamma}$ close to zero. After a set number of evaluations (here we found 4 to be a good value for convergence) in the gradient descent search, we update the target unitary coordinates \vec{c} and $\vec{\gamma}$ and refresh the L-BFGS memory, if changing the target introduces significant error.

We want to include the effect of additional leakage in order to obtain realistic control solutions. For each subsystem, we simulate three Transmon levels labeled $|0\rangle$, $|1\rangle$ and $|2\rangle$. To ensure that system dynamics stay within the embedded computational subspace, we write a running cost

$$L = \sum_k \sum_{\lambda \in \Lambda} |\langle \lambda | \psi(t_k) \rangle|^2 \quad (14)$$

and add it to the goal function. Population in the leakage levels $\Lambda = \{|0, 2\rangle, |1, 2\rangle, |2, 0\rangle, |2, 1\rangle\}$ is evaluated at evenly spaced times t_k during propagation.

In Fig. 4, we show the infidelities ϵ during optimization. Starting in a dispersive setting where $g/(\omega_2 - \omega_1) < 0.1$, we observe that optimizing for single-qubit gates trends towards isolated subsystems. When we target a perfect entangler, we observe convergence to a higher dispersivity, but still within the weak coupling regime. A combination of both goal functions, representing a single cell (Fig. 1) of some quantum computing algorithm, results in a compromise between the two edge cases, both in terms of dispersivity and reached fidelity. We also observe that the optimization trajectory in the "algorithm" target seems to be a superposition of the two layers. In this regime, the single-qubit gates can be realized to high fidelity, so the entangling and "algorithm" errors are close.

When initializing the system in the "straddling" regime, i.e. $g/(\omega_2 - \omega_1) = 0.1$ we find that we can recover the same convergence to single-qubit gates. After a short exploration, the entangling gates return to the same effective coupling value and perform slightly better than in the dispersive initialization. The optimization for both however seems to get stuck realizing a compromise. This regime has been shown to be optimal in the presence of arbitrary control, but here, the chosen simple parametrization might be not expressive enough to realize this potential.

B. Flux-tunable coupler

As seen in the previous section, choosing a fixed frequency, fixed coupling design limits fidelities of algo-

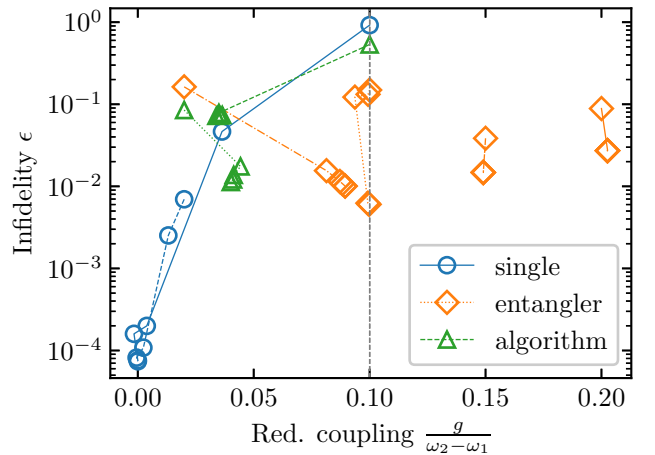


FIG. 4. **Model space of a fixed frequency, two-qubit chip.** We optimize the parameters of two Transmons, their frequencies, anharmonicities and coupling, to realize local and non-local gates. Initializing the search around the straddling regime (dashed line), $\omega_2 - \omega_1 = 500$ MHz 2π and for different values of $g = 50$ MHz 2π , we observe that local gates trend towards the same convergence. Only trajectories that converge below an error of 0.1 are shown.

gorithms, since the optimal parameter regimes for single and two-qubit operations are different. The introduction of tunable elements presents a solution, by allowing different working points for both tasks. In principle, there are two designs: Adding a flux line to one of the qubits to tune its resonance frequency or add a tunable coupler, another non-data qubit with a tunable frequency. However, the added flux lines also provide a new avenue for noise to degrade coherence time of the qubits. To compare to the fixed frequency setup in the previous section, we choose to investigate a tunable coupler architecture and assume that the added noise channel on the coupler qubit is reasonably isolated from the data qubits.

The flux-dependent frequency of a tunable element, is written as

$$\omega_i(\Phi) = (\omega_i^0 - \delta_i) \sqrt{\left| \cos\left(\frac{\Phi}{\Phi_0}\pi\right) \right|} + \delta_i \quad (15)$$

following the supplements of [22], where ω_i^0 is the sweet spot frequency and Φ the external flux. For simplicity, in this work we will directly consider the frequency offset $\omega_i^c(t)$ as the control parameter, such that $\omega_i = \omega_i^0 + \omega_i^c(t)$.

As a characteristic quantity, we look at the effective interaction strength

$$J = \frac{g_1 g_2}{2} \left(\frac{1}{\omega_1 - \omega_{\text{TC}}^0} + \frac{1}{\omega_2 - \omega_{\text{TC}}^0} \right) \quad (16)$$

induced between the two qubits [20]. Here, g_1 and g_2 being the coupling strength between qubit 1 and 2 and the coupler, respectively.

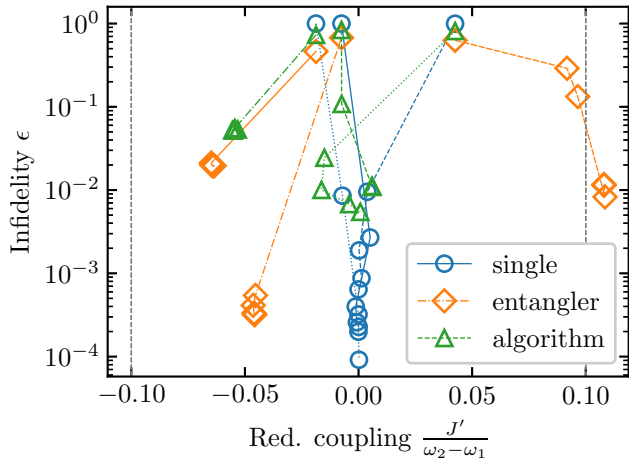


FIG. 5. **Adding a tunable coupler to the model.** When we initialize the system in a sweet spot, where, according to Eq. (16) the interaction between the qubits vanishes, good single-qubit gates can be reached. Entangling gates are trending towards effective couplings similar to the straddling regime. Optimizations starting in stronger coupling regimes have either stalled, or recovered to regions of weak coupling. Only trajectories that converge below an error of 0.1 are shown.

We put the idle point of the coupler ω_{TC}^0 above the qubits in Eq. (16), around the same difference in frequency

$$\omega_{TC}^0 - \omega_2 = \omega_2 - \omega_1. \quad (17)$$

If, in addition, there's a static coupling g_{12} between the qubits, the total effective interaction is

$$J' = g_{12} + \frac{g_1 g_2}{2} \left(\frac{1}{\omega_1 - \omega_{TC}^0} + \frac{1}{\omega_2 - \omega_{TC}^0} \right) \quad (18)$$

For g_1 and g_2 , we pick similar values to the coupling constant in the previous example, and we select the residual interaction g_{12} to initialize the optimization in different J' regimes. To entangle the qubits, we modulate ω_c with an AC tone close to their difference frequency [20], shaped by the same flattop envelopes as before. Again, we can realize single and entangling gates to good fidelities. Single-qubit gates can reach good fidelities here, even exploring the region around the sweet spot and returning. Once the interaction strength is high enough, we can also entangle the qubits with a higher fidelity than the case without the tunable coupler. For the "algorithm" optimization, the same competition between local and non-local operations results in a stagnation at sub-par fidelity. The trajectory of the combined case is again alternating between the individual trajectories, see Fig. 5.

In both cases, we see that the approaching the strong coupling regime presents problems in realizing single-

qubit gates, at least with the simple pulse shapes we explored here.

IV. SUMMARY AND OUTLOOK

We have shown a general procedure to investigate model design space for an application like superconducting qubits, where the properties of human-made devices can be targeted in fabrication. Instead of a full optimal control approach, we investigate if previous results about preferable regimes hold for simple pulse shapes. Compared to previous work, we choose a direct search in the Weyl space to find the closest perfect entangler to the gate our test system can produce. This way, we avoid some mathematical difficulties, since the expression of the functional Eq. (3) is only defined outside the volume. Inside the volume, the value is 1 by definition. The direct use of Eq. (7) does not require these conditional expressions.

The application to the two-qubit model, optionally adding a tunable coupler, shows reliably that good single-qubit gates can be reached when the effective interaction is turned almost off. This is as expected but also holds, when initializing a search some distance away from this regime. By the same reasoning, targeting entangling gates trends towards a similar point – the previously identified "straddling" regime from different initial values. There, we notice the necessity to restart optimizations, in the case of early termination. The use of simple pulses seems to limit the exploration of parameter space and prevents a good regime for the operation of both local and non-local quantum gates. To make a more systematic claim, a wider range of cases – control schemes and device designs – needs to be tested. For example, several schemes exist to mitigate the effect of spurious ZZ interactions to allow single-qubit control on more strongly interacting systems [23, 24].

Even limited to the superconducting platform, several design paradigms to realize quantum computing devices exist. The Transmon, with its specific E_C/E_J ratio, is only one possible design. It is the qubit design most demonstrations of applied quantum computing use. There are other promising paradigms, such as the Fluxonium, which combines insensitivity to external noise with a large anharmonicity [25]. So, a different search space can be explored with the method presented here by directly optimizing Josephson junctions, capacitances and inductances.

V. ACKNOWLEDGEMENTS

We thank our colleagues, particularly A. Mishra, for discussion and comments on the manuscript.

This work is supported by funding from the German Federal Ministry of Education and Research via the funding program quantum technologies – from basic research to the market – under contract numbers 13N15680 "GeQ-CoS".

-
- [1] P. Krantz, M. Kjaergaard, F. Yan, T. P. Orlando, S. Gustavsson, and W. D. Oliver, *Applied Physics Reviews* **6**, 021318 (2019), arXiv:1904.06560 [cond-mat, physics:physics, physics:quant-ph].
- [2] J. Kunasaikaran, K. Mato, and R. Wille, *A Framework for the Design and Realization of Alternative Superconducting Quantum Architectures* (2023), arXiv:2305.07052 [quant-ph].
- [3] X. Ni, H.-H. Zhao, L. Wang, F. Wu, and J. Chen, *npj Quantum Information* **8**, 7 (2022).
- [4] T. Rajabzadeh, A. Boulton-McKeehan, S. Bonkowsky, D. I. Schuster, and A. H. Safavi-Naeini, *A General Framework for Gradient-Based Optimization of Superconducting Quantum Circuits using Qubit Discovery as a Case Study* (2024), arXiv:2408.12704 [cond-mat, physics:physics, physics:quant-ph].
- [5] C. Guinn, S. Stein, E. Tureci, G. Avis, C. Liu, S. Krastanov, A. A. Houck, and A. Li, *Co-Designed Superconducting Architecture for Lattice Surgery of Surface Codes with Quantum Interface Routing Card* (2023), arXiv:2312.01246 [quant-ph].
- [6] T. Menke, F. Häse, S. Gustavsson, A. J. Kerman, W. D. Oliver, and A. Aspuru-Guzik, *npj Quantum Information* **7**, 8 (2021).
- [7] K. X. Wei, I. Lauer, E. Pritchett, W. Shanks, D. C. McKay, and A. Javadi-Abhari, *Native two-qubit gates in fixed-coupling, fixed-frequency transmons beyond cross-resonance interaction* (2023), arXiv:2310.12146 [quant-ph].
- [8] M. H. Goerz, G. Gualdi, D. M. Reich, C. P. Koch, F. Motzoi, K. B. Whaley, J. Vala, M. M. Müller, S. Montangero, and T. Calarco, *Physical Review A* **91**, 10.1103/physreva.91.062307 (2015).
- [9] S. F. Lin, S. Sussman, C. Duckering, P. S. Mundada, J. M. Baker, R. S. Kumar, A. A. Houck, and F. T. Chong, *Let Each Quantum Bit Choose Its Basis Gates* (2022), arXiv:2208.13380 [quant-ph].
- [10] P. Kairys and T. S. Humble, in *2021 IEEE International Conference on Quantum Computing and Engineering (QCE)* (IEEE, Broomfield, CO, USA, 2021) pp. 413–418.
- [11] Google AI Quantum, B. Foxen, C. Neill, A. Dunsworth, P. Roushan, B. Chiaro, A. Megrant, J. Kelly, Z. Chen, K. Satzinger, R. Barends, F. Arute, K. Arya, R. Babush, D. Bacon, J. C. Bardin, S. Boixo, D. Buell, B. Burkett, Y. Chen, R. Collins, E. Farhi, A. Fowler, C. Gidney, M. Giustina, R. Graff, M. Harrigan, T. Huang, S. V. Isakov, E. Jeffrey, Z. Jiang, D. Kafri, K. Kechedzhi, P. Klimov, A. Korotkov, F. Kostritsa, D. Landhuis, E. Lucero, J. McClean, M. McEwen, X. Mi, M. Mohseni, J. Y. Mutus, O. Naaman, M. Neeley, M. Niu, A. Petukhov, C. Quintana, N. Rubin, D. Sank, V. Smelyanskiy, A. Vainsencher, T. C. White, Z. Yao, P. Yeh, A. Zalcman, H. Neven, and J. M. Martinis, *Physical Review Letters* **125**, 120504 (2020).
- [12] F. Setiawan, P. Groszkowski, and A. A. Clerk, *Physical Review Applied* **19**, 034071 (2023).
- [13] M. H. Goerz, F. Motzoi, K. B. Whaley, and C. P. Koch, *npj Quantum Information* **3**, 1 (2017).
- [14] L. DiCarlo, J. M. Chow, J. M. Gambetta, L. S. Bishop, B. R. Johnson, D. I. Schuster, J. Majer, A. Blais, L. Frunzio, S. M. Girvin, and R. J. Schoelkopf, *Nature* **460**, 240 (2009).
- [15] J. M. Chow, A. D. Córcoles, J. M. Gambetta, C. Rigetti, B. R. Johnson, J. A. Smolin, J. R. Rozen, G. A. Keefe, M. B. Rothwell, M. B. Ketchen, and M. Steffen, *Physical Review Letters* **107**, 080502 (2011).
- [16] J. Ghosh, A. Galiutdinov, Z. Zhou, A. N. Korotkov, J. M. Martinis, and M. R. Geller, *Physical Review A* **87**, 022309 (2013).
- [17] Y. Makhlin, *Quantum Information Processing* **1**, 10.1023/A:1022144002391 (2002).
- [18] P. Watts, J. Vala, M. M. Müller, T. Calarco, K. B. Whaley, D. M. Reich, M. H. Goerz, and C. P. Koch, *Physical Review A* **91**, 10.1103/physreva.91.062306 (2015).
- [19] J. Zhang, J. Vala, S. Sastry, and K. B. Whaley, *Physical Review A* **67**, 042313 (2003).
- [20] D. C. McKay, S. Filipp, A. Mezzacapo, E. Magesan, J. M. Chow, and J. M. Gambetta, *Physical Review Applied* **6**, 064007 (2016).
- [21] F. Motzoi, J. M. Gambetta, P. Rebentrost, and F. K. Wilhelm, *Physical Review Letters* **103**, 10.1103/physrevlett.103.110501 (2009).
- [22] M. A. Rol, F. Battistel, F. K. Malinowski, C. C. Bultink, B. M. Tarasinski, R. Vollmer, N. Haider, N. Muthusubramanian, A. Bruno, B. M. Terhal, and L. DiCarlo, *Physical Review Letters* **123**, 120502 (2019).
- [23] P. Mundada, G. Zhang, T. Hazard, and A. Houck, *Physical Review Applied* **12**, 054023 (2019).
- [24] A. Kandala, K. X. Wei, S. Srinivasan, E. Magesan, S. Carnevale, G. A. Keefe, D. Klaus, O. Dial, and D. C. McKay, *Physical Review Letters* **127**, 130501 (2021).
- [25] F. Bao, H. Deng, D. Ding, R. Gao, X. Gao, C. Huang, X. Jiang, H.-S. Ku, Z. Li, X. Ma, X. Ni, J. Qin, Z. Song, H. Sun, C. Tang, T. Wang, F. Wu, T. Xia, W. Yu, F. Zhang, G. Zhang, X. Zhang, J. Zhou, X. Zhu, Y. Shi, J. Chen, H.-H. Zhao, and C. Deng, *Physical Review Letters* **129**, 010502 (2022).